AN ADAPTIVE INTEGRATION SCHEME IN COMPUTATIONAL INELASTICITY

Reijo KOUHIA[1] and Marcus RÜTER[2]

[1] Helsinki University of Technology, Structural Mechanics, PO Box 2100, FIN-02015 TKK
[2] Helsinki University of Technology, Institute of Mathematics, PO Box 1100, FIN-02015 TKK

ABSTRACT

In this paper, an adaptive approach based on a time discontinuous Galerkin method (dG) is proposed. For large time steps and in a linear non-autonomous case, it reduces to the asymptotically second-order accurate Lobatto IIIC type implicit Runge-Kutta method, which is equal to the Padé-(0,2) approximation of the exponential function. In the asymptotic range it will result in the asymptotically third-order accurate scheme, the dG(1) method.

Accuracy and efficiency of the proposed method are studied in detail for common models in creep and plasticity. Comparisons are made to the commonly used backward Euler scheme which is known to give accurate results for large time steps.

1 INTRODUCTION

There are many different algorithms for the integration of inelastic constitutive models. However, the fully implicit backward Euler scheme seems to be the most popular, although it is asymptotically only first-order accurate [1, 2, 3]. In analysing practical problems, especially in creep analysis and viscoplasticity, the time steps to be used are often large, several magnitudes larger than the critical time step of some explicit methods, e.g. the forward Euler method. Therefore, the integrator should be unconditionally stable and sufficiently accurate for large time steps.

As shown in [4], the asymptotic convergence rate does not necessarily reflect high accuracy outside the asymptotic range, which is usually step sizes smaller than the critical time step of the explicit Euler method. The asymptotically first-order accurate implicit Euler method seems to be more accurate than many asymptotically higher-order schemes for large time steps. Therefore, an integrator for inelastic constitutive models should be at least [4]:

1. L-stable
2. for $\dot{\sigma} + \lambda\sigma = 0$ (λ = constant), the amplification factor should be
   (a) strictly positive, and
   (b) monotonous (convex).

It is obvious that the standard backward Euler scheme fulfills these requirements.

The discontinuous Galerkin family of methods seem rather ideal for the integration of inelastic constitutive models. However, they have some shortcomings, as explaned in [4].

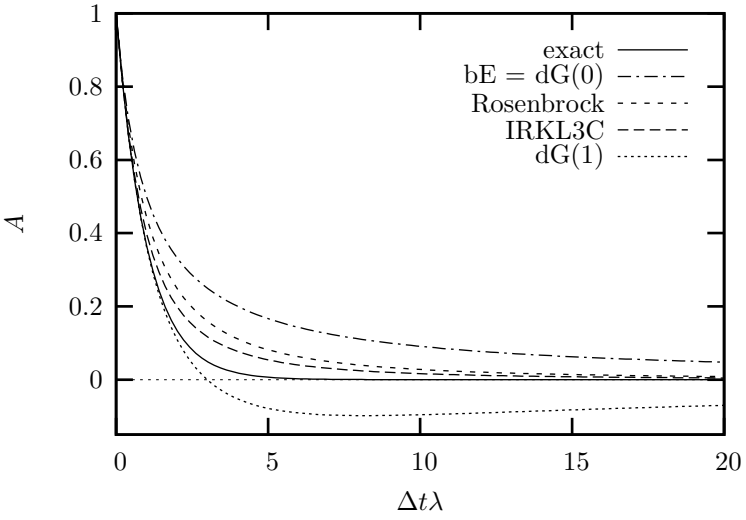

Figure 1: Amplification factors of different time integrators.

The second-order accurate two-stage Lobatto IIIC type implicit Runge-Kutta method (IRKL3C) exhibits good accuracy properties also for large time steps. When the integrals in the dG(1) scheme are underintegrated by using the two-point Gauss-Lobatto scheme (endpoint rule) the dG(1) scheme is identical to the IRKL3C-scheme [5]. The dG(0) and dG(1) schemes have been used in elastoplasticity by Alberty and Carstensen [6, 7]. In [8] the first-order accurate Rosenbrock method is recommended to inviscid plasticity computations.

The amplification factors applied to the linear scalar problem $\dot{\sigma} + \lambda\sigma = 0$ are shown for certain integrators in Fig. 1.

2 NUMERICAL INTEGRATION

In this section, the basic equations of discontinuous Galerkin and implicit Runge-Kutta methods are described. More details can be found in [10, 11].

2.1 The discontinuous Galerkin method

The following evolution problem will be considered:

$$\dot{\boldsymbol{\sigma}} = \boldsymbol{f}(\boldsymbol{\sigma}), \tag{1}$$

where $\boldsymbol{f}$ is some function of the stress $\boldsymbol{\sigma}$. The discontinuous Galerkin method of degree q can be stated as: in a time interval $I_n = (t_n, t_{n+1}]$ find $\boldsymbol{\sigma}$ (polynomial of degree q) such that

$$\int_{I_n} (\dot{\boldsymbol{\sigma}} - \boldsymbol{f}(\boldsymbol{\sigma})) : \boldsymbol{\tau} \, \mathrm{d}t + [\![\boldsymbol{\sigma}_n]\!] : \boldsymbol{\tau}_n^+ = 0. \tag{2}$$

For the test functions $\boldsymbol{\tau}$, polynomials of degree q are used. The notations $\boldsymbol{\sigma}_n^+$ and $\boldsymbol{\sigma}_n^-$ are the limits $\boldsymbol{\sigma}_n^\pm = \lim_{\epsilon\to 0} \boldsymbol{\sigma}(t_n \pm |\epsilon|), [\![\boldsymbol{\sigma}_n]\!] = \boldsymbol{\sigma}_n^+ - \boldsymbol{\sigma}_n^-$. These notations are illustrated in Fig. 2.

The discontinuous Galerkin method allows the use of piecewise constant trial and test functions. In this case, $\tau_{ij} = 1$ and $\boldsymbol{\sigma}$ is constant on the time step n and the dG(0) method

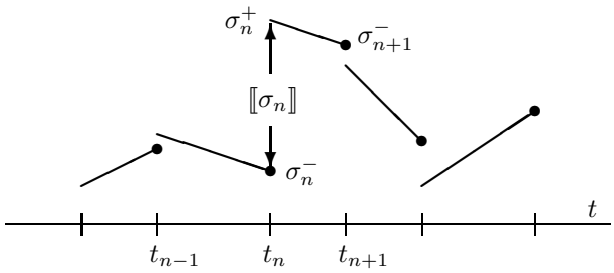

Figure 2: Discontinuous Galerkin method, dG(1); notation.

can be stated as follows

$$\boldsymbol{\sigma}_{n+1} - \int_{I_n} \boldsymbol{f}(\boldsymbol{\sigma}_{n+1})\ \mathrm{d}t = \boldsymbol{\sigma}_n, \tag{3}$$

where $\boldsymbol{\sigma}_{n+1} = \boldsymbol{\sigma}_{n+1}^- = \boldsymbol{\sigma}_n^+$, and $\boldsymbol{\sigma}_n = \boldsymbol{\sigma}_n^-$. If the function $\boldsymbol{f}$ is linear in the stress, i.e $\boldsymbol{f} = \boldsymbol{f}_0 - \mathbb{A} : \boldsymbol{\sigma}$, where $\boldsymbol{f}_0, \mathbb{A}$ are second- and fourth-order tensors independent of the stress, the dG(0) method can be written as:

$$(\mathbb{I} + \tilde{\mathbb{A}}_{n+1}) : \boldsymbol{\sigma}_{n+1} = \boldsymbol{\sigma}_n + \int_{I_n} \boldsymbol{f}_0\ \mathrm{d}t, \tag{4}$$

where

$$\tilde{\mathbb{A}}_{n+1} = \int_{I_n} \mathbb{A}\ \mathrm{d}t \tag{5}$$

and $\mathbb{I}$ is the fourth-order identity tensor. For constant $\mathbb{A}$ and without the source term ($\boldsymbol{f}_0 = \boldsymbol{0}$), the dG(0) method is identical to the implicit backward Euler scheme.

2.2 Implicit Runge-Kutta methods

There is a close connection between the implicit Runge-Kutta (IRK) and discontinuous Galerkin methods. The discontinuous Galerkin method of degree q, dG(q), is equivalent to the $q+1$-stage Radau IIA type IRK-method, which is of order $2q-1$. Their amplification factors are the $(q, q+1)$ subdiagonal Padé approximations of $\exp(-\lambda\Delta t)$ and the methods are L-stable.

An s-stage implicit Runge-Kutta method for the solution of the evolution equation (1) can be defined as

$$\boldsymbol{k}_i = \boldsymbol{\sigma}_n + \Delta t \sum_{j=1}^{s} a_{ij} \boldsymbol{f}(t_n + c_j \Delta t, \boldsymbol{k}_j) \qquad i = 1, \ldots, s \tag{6}$$

$$\boldsymbol{\sigma}_{n+1} = \boldsymbol{\sigma}_n + \Delta t \sum_{j=1}^{s} b_j \boldsymbol{f}(t_n + c_j \Delta t, \boldsymbol{k}_j). \tag{7}$$

For the third order accurate two stage Radau IIA method, the coefficients have the values $a_{11} = 5/12, a_{21} = 3/4, a_{12} = -1/12, a_{22} = 1/4, c_1 = 1/3, c_2 = 1, b_1 3/4, b_2 = 1/4$. This scheme is equal to the dG(1)-method. If the dG(1)-method is integrated by the two-point Gauss-Lobatto rule, is it equal to the second order accurate two stage Lobatto IIIC method, which have the following values for the coefficients: $a_{11} = a_{21} = a_{22} = -a_{12} = 1/2, c_1 = 0, c_2 = 1, b_1 = b_2 = 1/2$.

3 SMALL STRAIN ELASTOPLASTICITY

Next, we briefly present the small strain elastoplasticity problem. The isotropic elastoplastic body is given by the closure of a bounded open set $\Omega \subset \mathbb{R}^3$ with a piecewise smooth, polyhedral and Lipschitz continuous boundary Γ such that $\Gamma = \bar{\Gamma}_D \cup \bar{\Gamma}_N$ and $\Gamma_D \cap \Gamma_N = \emptyset$, where Γ_D and Γ_N are the portions of the boundary Γ where Dirichlet and Neumann boundary conditions are imposed, respectively.

Due to the assumed additive decomposition of the total strain tensor $\boldsymbol{\varepsilon} = \operatorname{sym} \operatorname{grad} \boldsymbol{u}$ into an elastic part $\boldsymbol{\varepsilon}^{\mathrm{e}}$ and a plastic part $\boldsymbol{\varepsilon}^{\mathrm{p}}$, the elastic strains can be determined by

$$\boldsymbol{\varepsilon}^{\mathrm{e}} = \boldsymbol{\varepsilon} - \boldsymbol{\varepsilon}^{\mathrm{p}}. \tag{8}$$

From the dissipation inequality we then infer the constitutive relation

$$\boldsymbol{\sigma} = \frac{\partial W}{\partial \boldsymbol{\varepsilon}^{e}} \tag{9}$$

with stress tensor $\boldsymbol{\sigma}$ and specific strain-energy function $W = \frac{1}{2}\boldsymbol{\varepsilon}^{\mathrm{e}} : \mathbb{C}^{\mathrm{e}} : \boldsymbol{\varepsilon}^{\mathrm{e}}$, where we introduced the elasticity tensor

$$\mathbb{C}^{\mathrm{e}} = \varkappa \mathbf{1} \otimes \mathbf{1} + 2\mu \mathbb{P}. \tag{10}$$

Here, $\varkappa$ denotes the bulk modulus, μ is a Lamé parameter, $\mathbf{1}$ is the second-order identity tensor and $\mathbb{P}$ is the fourth-order projection tensor defined as $\mathbb{P} = \mathbb{I} - \frac{1}{3}\mathbf{1} \otimes \mathbf{1}$.

In order to determine the elastic strains (8) and thus the stresses (9) we need to determine the plastic strains. Therefore, we next introduce the yield function $\Phi = \Phi(\boldsymbol{\sigma})$ which defines the closed and convex set

$$\bar{\mathcal{E}} = \{\boldsymbol{\sigma} \,:\, \Phi(\boldsymbol{\sigma}) \leq 0\} \tag{11}$$

in stress space. The interior $\mathcal{E}$ of this set is called the elastic domain, whereas the boundary $\partial\mathcal{E}$ is called the yield surface. In this paper, we restrict our considerations to the case of von-Mises plasticity as used to model, e.g., steel structures. In this case, the yield function is defined as

$$\Phi(\boldsymbol{\sigma}) = \| \operatorname{dev} \boldsymbol{\sigma} \| - \sqrt{\frac{2}{3}} y_0 \tag{12}$$

with yield stress y_0 and "dev" denoting the deviator.

From the principle of maximum dissipation we then obtain the associative flow rule

$$\dot{\boldsymbol{\varepsilon}}^{\mathrm{p}} = \lambda \boldsymbol{n} \tag{13}$$

and the Kuhn-Tucker conditions, also referred to as loading and unloading conditions,

$$\lambda \geq 0 \quad ; \quad \Phi(\boldsymbol{\sigma}) \leq 0 \quad ; \quad \lambda \Phi(\boldsymbol{\sigma}) = 0. \tag{14}$$

In the above, $\boldsymbol{n}$ is the normal defined as $\boldsymbol{n} = \partial\Phi(\boldsymbol{\sigma})/\partial\boldsymbol{\sigma}$ and λ is the plastic parameter. In the special case of von-Mises plasticity we obtain $\boldsymbol{n} = \operatorname{dev}\boldsymbol{\sigma}/\| \operatorname{dev}\boldsymbol{\sigma}\|$ and $\lambda = \boldsymbol{n} : \dot{\boldsymbol{\varepsilon}}$.

In order to determine the plastic flow and thus the stresses at the end of the time step I_n, we make use of the well-known operator split technique, i.e. we split the problem into an elastic predictor and a plastic corrector step.

In the elastic predictor step we assume that no plastic flow appears. Hence, we solve the initial value problem

$$\dot{\boldsymbol{\varepsilon}} = \dot{\boldsymbol{\varepsilon}}^{\mathrm{e,trial}} \tag{15}$$

$$\dot{\boldsymbol{\varepsilon}}^{\mathrm{p}} = \boldsymbol{0} \tag{16}$$

subjected to the initial condition

$$\boldsymbol{\varepsilon}_n^{\mathrm{e},+} = \boldsymbol{\varepsilon}_n^{\mathrm{e,trial},+} \tag{17}$$

for the trial strains $\boldsymbol{\varepsilon}_{n+1}^{\mathrm{e,trial},-}$. The notations are illustrated in Fig. 2.

Integrating (15) over the time interval I_n yields

$$\int_{I_n} \dot{\boldsymbol{\varepsilon}} \, \mathrm{d}t = \int_{I_n} \dot{\boldsymbol{\varepsilon}}^{\mathrm{e,trial}} \, \mathrm{d}t \tag{18}$$

and thus

$$\boldsymbol{\varepsilon}_{n+1}^{-} - \boldsymbol{\varepsilon}_n^{+} = \boldsymbol{\varepsilon}_{n+1}^{\mathrm{e,trial},-} - \boldsymbol{\varepsilon}_n^{\mathrm{e,trial},+}. \tag{19}$$

With the initial condition (17), the exact solution reads

$$\boldsymbol{\varepsilon}_{n+1}^{\mathrm{e,trial}-} = \boldsymbol{\varepsilon}_{n+1}^{-} - \boldsymbol{\varepsilon}_n^{\mathrm{p},+}. \tag{20}$$

Clearly, the stresses at the end of the time interval I_n can then be computed as

$$\boldsymbol{\sigma}_{n+1}^{\mathrm{trial},-} = \mathbb{C}^{\mathrm{e}} : \boldsymbol{\varepsilon}_{n+1}^{\mathrm{e,trial}-}. \tag{21}$$

If the trial stresses are element of $\bar{\mathcal{E}}$, then no plastic flow appears and thus no plastic corrector step is required. If, however, the yield condition is not satisfied by the trial stresses $\boldsymbol{\sigma}_{n+1}^{\mathrm{trial},-}$, then we have to solve the following initial value problem, also referred to as the plastic corrector step,

$$\dot{\boldsymbol{\varepsilon}} + \dot{\boldsymbol{\varepsilon}}^{\mathrm{e,trial}} = \boldsymbol{0} \tag{22}$$

$$\dot{\boldsymbol{\varepsilon}}^{\mathrm{p}} = \lambda \boldsymbol{n} \tag{23}$$

subjected to the initial condition

$$\boldsymbol{\varepsilon}_{n+1}^{\mathrm{e},+} = \boldsymbol{\varepsilon}_n^{\mathrm{e,trial},-} \tag{24}$$

and the Kuhn-Tucker conditions (14).

The associated discontinuous Galerkin method dG(q) of polynomial order q (in terms of stresses) then reads: find a solution $\boldsymbol{\sigma}_{n+1}^{-}$ such that

$$b_n(\dot{\boldsymbol{\sigma}}, \boldsymbol{\tau}) + \boldsymbol{\sigma}_n^{+} : \boldsymbol{\tau}_n^{+} = -c_n(\boldsymbol{\sigma}, \boldsymbol{\tau}) + \boldsymbol{\sigma}_n^{-} : \boldsymbol{\tau}_n^{+} \tag{25}$$

with the bilinear form

$$b_n(\boldsymbol{\sigma}, \boldsymbol{\tau}) = \int_{I_n} \boldsymbol{\sigma} : \boldsymbol{\tau} \, \mathrm{d}t \tag{26}$$

and the semi-linear form (i.e. it is linear only with respect to its second argument)

$$c_n(\boldsymbol{\sigma}, \boldsymbol{\tau}) = \int_{I_n} \lambda \boldsymbol{n} : \mathbb{C}^{\mathrm{e}} : \boldsymbol{\tau} \, \mathrm{d}t \,. \tag{27}$$

In the special case where $q = 0$, i.e. for piecewise constant functions in time, we can set $\tau_{ij} = 1$ and thus the dG-method (25) reduces to

$$\boldsymbol{\sigma}_n^{+} = -\int_{I_n} \lambda \boldsymbol{n} : \mathbb{C}^{\mathrm{e}} \, \mathrm{d}t + \boldsymbol{\sigma}_n^{-}. \tag{28}$$

Consequently, the stresses at the end of the time interval I_n can be determined by

$$\boldsymbol{\sigma}_{n+1}^{-} = -\Delta t_n \lambda \boldsymbol{n} : \mathbb{C}^{\mathrm{e}} + \boldsymbol{\sigma}_{n+1}^{\mathrm{trial},-}, \tag{29}$$

where Δt_n is the length of the time interval I_n. Evaluating $\boldsymbol{n}$ at the end of the time interval, the classical backward Euler scheme

$$\boldsymbol{\sigma}_{n+1}^{-} = -\Delta t_n \lambda_{n+1} \boldsymbol{n}_{n+1} : \mathbb{C}^{\mathrm{e}} + \boldsymbol{\sigma}_{n+1}^{\mathrm{trial},-} \tag{30}$$

can be recovered.

In the case where $q \geq 1$, we first have to linearise the nonlinear variational problem (25) which yields the linearised problem of solving

$$b_n(\boldsymbol{\Delta\dot{\sigma}}, \boldsymbol{\tau}) + c_{n,\sigma}(\boldsymbol{\Delta\sigma}, \boldsymbol{\tau}) = -b_n(\boldsymbol{\dot{\sigma}}, \boldsymbol{\tau}) - c_n(\boldsymbol{\sigma}, \boldsymbol{\tau}) - \boldsymbol{\sigma}_n^{+} : \boldsymbol{\tau}_n^{+} + \boldsymbol{\sigma}_{n+1}^{\mathrm{trial},-} : \boldsymbol{\tau}_n^{+} \tag{31}$$

for a stress increment $\boldsymbol{\Delta\sigma}$. In the special case of von-Mises plasticity, the bilinear form $c_{n,\sigma}$ is given as

$$c_{n,\sigma}(\boldsymbol{\Delta\sigma}, \boldsymbol{\tau}) = \int_{I_n} \boldsymbol{\Delta\sigma} : \left[\left(\frac{\partial \boldsymbol{n}}{\partial \boldsymbol{\sigma}} : \dot{\boldsymbol{\varepsilon}} \right) \otimes (\boldsymbol{n} : \mathbb{C}^{\mathrm{e}}) \right] : \boldsymbol{\tau} + \lambda \boldsymbol{\Delta\sigma} : \frac{\partial \boldsymbol{n}}{\partial \boldsymbol{\sigma}} : \mathbb{C}^{\mathrm{e}} : \boldsymbol{\tau} \, \mathrm{d}t, \tag{32}$$

where it was used that

$$\frac{\partial \lambda}{\partial \boldsymbol{\sigma}} = \frac{\partial \boldsymbol{n}}{\partial \boldsymbol{\sigma}} : \dot{\boldsymbol{\varepsilon}} \tag{33}$$

with

$$\frac{\partial \boldsymbol{n}}{\partial \boldsymbol{\sigma}} = \| \operatorname{dev} \boldsymbol{\sigma} \|^{-1} \left(\mathbb{P} - \boldsymbol{n} \otimes \boldsymbol{n} \right). \tag{34}$$

Clearly, the exact solution should be continuous in time. Hence, the jump in the time discretization at the end of each time interval I_n can be used to estimate the error in the time discretization. Consequently, it becomes possible to refine the time mesh adaptively based on the jumps at the end of I_n.

4 NUMERICAL EXAMPLES

In a uniaxial case and using the Garofalo type creep model [12], the evolution equation for the stress (1) has the form

$$\dot{\sigma} = E \left[\dot{\varepsilon} - f^* \exp\left(-Q/R\theta\right) \sinh^m \left(\sigma/\sigma_{\mathrm{r}}\right) \right], \tag{35}$$

where E is the Young's modulus, f^* the fluidity parameter, Q the process activation energy, R the gas constant, θ the absolute temperature and σ_{r} is the "flow stress" stress. In this example, the exponent m and the coefficient f^* are assumed to be constant, although they depend on the grain size [12].

Thermally softening and hardening cases have been studied, although the results are only presented from the softening case since the behaviour of the integrators is similar for both cases. The temperature is assumed to change linearly with time $\theta(t) = \theta_0 \pm \Delta\theta(t/t_{\max})$, and $\theta_0 = 293$ K, $\Delta\theta = 40$ K. Increase or decrease in temperature result in softening or hardening behaviour, respectively. The material parameters used correspond to the binary near eutectic Sn40Pb solder and are the following [13]: $E = 33$ GPa, $Q = 12$ kcal/mol, $R = 2{\cdot}10^{-3}$ kcal/mol·K, $\sigma_y = 20$ MPa, $f = 10^5$ s^{-1}, $m = 3.5$.

The behaviour of the dG(1), with two-point Gauss-Legendre integration, the underintegrated dG(1), with two-point Gauss-Lobatto integration, abbreviated as dG(1)-Lobatto, the two stage IRKL3C-scheme and the backward Euler (bE) methods are studied numerically using two loading patterns; a constant strain rate loading ($\varepsilon = \dot{\varepsilon}_0 t$, $\dot{\varepsilon}_0 = 10^{-5}$ 1/s) and a pulsatile cyclic straining, see Fig. 3. As shown in [4, 5] the behaviour of the dG(0)-scheme is inferior as compared to the backward Euler method, hence the results of the dG(0) are not shown here.

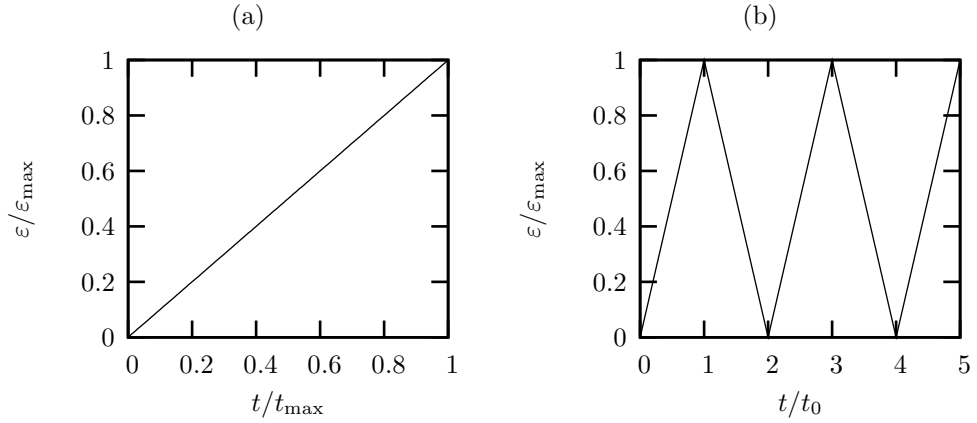

Figure 3: Loading types: (a) constant strain-rate loading $\dot{\varepsilon} = 10^{-5}$ s^{-1}, $\varepsilon_{\max} = 0.01$, $t_{\max} = 1000$ s, (b) pulsatile loading with alternating strain-rates $\dot{\varepsilon} = \pm 10^{-5}$ s^{-1}, $\varepsilon_{\max} = 0.001$, $t_0 = 100$ s.

It can be seen from Fig. 4 that the IRKL3C method is equivalent to the dG(1) method with two point Lobatto integration at the endpoints of the steps. The dG(1) largely overshoots the stress at the end of the first step. However, the linear dG(1) solution is clearly a good approximation in an average sense over the time step. At the strain 0.01 (after the fifth step) the relative error in stress is 0.16 % for the dG(1) method and only 0.02 % for the IRK3LC and dG(1)-Lobatto methods.

It can also be seen from the figure that the backward Euler-scheme perform well in the second, fully inelastic step. Therefore, the most disasterous case for the bE-scheme seems to be a cyclic loading with repeated changes from elastic to inelastic states. In Fig. 5 the results of a pulsatile uniaxial straining case are shown. A large time-step, $\Delta t = t_0 = 100$ s is used. Convergence of the error at the end of loading, $t = t_{\max} = 5t_0$, is shown in Fig. 6; linear, quadratic and cubic rate of convergence in the asymptotic range is clearly visible for the bE, dG(1)-Lobatto and dG(1) methods, respectively. As expected for large step sizes, the underintegrated dG(1) is the most accurate.

5 CONCLUDING REMARKS

Formulation of the symptotically third order accurate dG(1)-scheme for small strain plasticity and creep-type inelastic models is presented. It is also shown that underintegrating the coefficients in the dG(1)-method by the two-point Gauss-Lobatto quadrature results in a quadratically convergent scheme, which has improved accuracy properties for large step sizes, even better than the popular first order accurate backward Euler scheme. The underintegrated dG(1)-method is shown to be equal to the two-stage Lobatto IIIC type implicit Runge-Kutta method.

Further investigations for the dG(1)-type schemes are needed to relate the jump in the stress to a proper error indicator. Also design of a switching strategy to change the quadrature from Gauss-Lobatto to Gauss-Legendre to obtain maximal accuracy for all step sizes is under development.

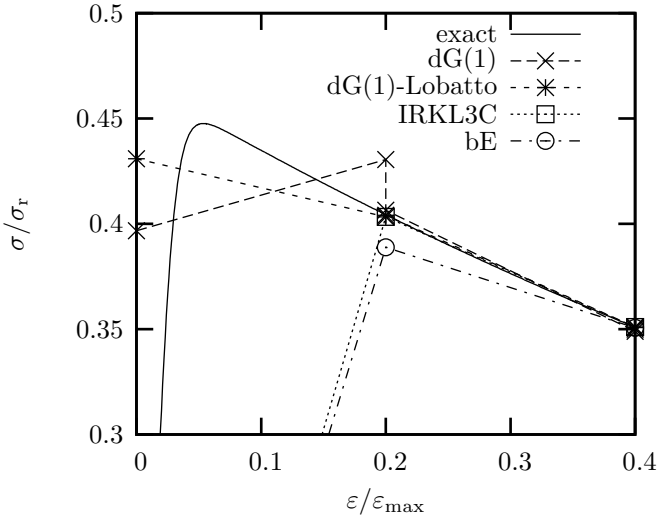

Figure 4: Uniaxial straining, strain rate 10^{-5} s^{-1}.

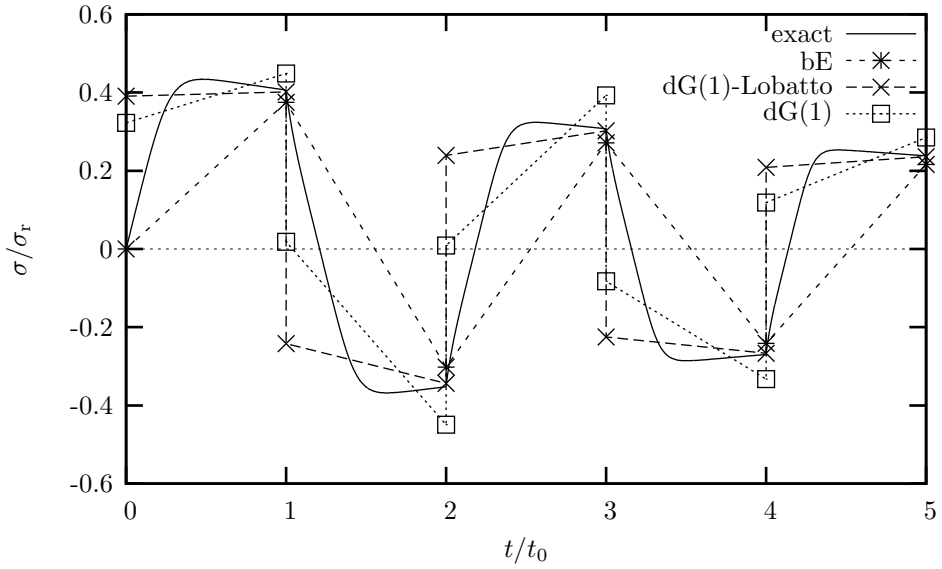

Figure 5: Pulsatile uniaxial straining, strain rate $\pm 10^{-5}$ s^{-1}.

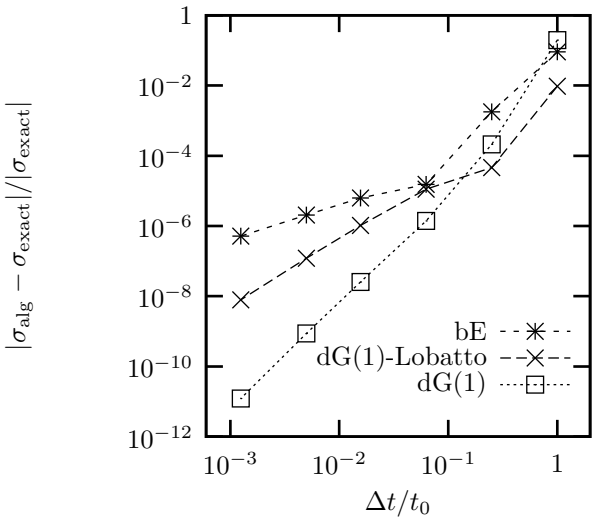

Figure 6: Relative error after five pulses as a function of time step.

ACKNOWLEDGEMENTS

This research has been supported in part by Tekes - the National Technology Agency of Finland (project KOMASI, decision number 40288/05) and by the DFG (German Research Foundation) under grant number Ru1213/1-1.

REFERENCES

[1] J.C. Simo and T.J.R. Hughes. *Computational Inelasticity*. Springer: New York, 1998.

[2] M. Wallin and M. Ristinmaa. *Accurate stress updating algorithm based on constant strain rate assumption.* Comp. Meth. Appl. Mech. Eng. **190** (42), 5583–5601 (2001)

[3] K. Runesson, S. Sture, K. Willam. *Integration in computational plasticity.* Comp. Struct., **30** (1/2), 119–130 (1988).

[4] R. Kouhia, P. Marjamäki, J. Kivilahti. *On the implicit integration of rate-dependent inelastic constitutive models*, Int. J. Numer. Meth. Engng., **62**, 1832–1856 (2005).

[5] R. Kouhia. *A time discontinuous Petrov-Galerkin method for the integration of inelastic constitutive equations*, In P. Neittaanmäki, T. Rossi, K. Majava and O. Pironneau (eds.) ECCOMAS 2004 CD-ROM proceedings.

[6] J. Alberty, C. Carstensen. *Numerical analysis of time-dependent primal elastoplasticity with hardening*, SIAM J. Numer. Anal., **37** (4), 1271–1294 (2000).

[7] J. Alberty, C. Carstensen. *Discontinuous Galerkin time discretization in elastoplasticity: motivation, numerical algorithms, and applications.* Comp. Meth. Appl. Mech. Eng., **191**, 4949–4969 (2002).

[8] K. Hackl, M. Schmidt-Baldassari. *Time integration algorithms for evolution equations in finite strain plasticity.* In W.A.. Wall et al., editors, *Trends in Computational Structural Mechanics*, pages 128–139, CIMNE, Barcelona, (2001).

[9] M. Schmidt-Baldassari, K. Hackl. *Advanced time integration algorithms for rate independent finite strain elastoplasticity.* Preprint 03-1, Ruhr-Universität Bochum, Lehrstuhl für Allgemeine mechanik, (2003).

[10] K. Eriksson, D. Estep, P. Hansbo, C. Johnsson. *Computational Differential Equations.* Studentlitteratur, 1996.

[11] E. Hairer, G. Wanner. *Solving Ordinary Differential Equations II, Stiff and Differential-Algebraic Problems.* Springer, second ed., 1991.

[12] F. Garofalo. *Fundamentals of Creep and Creep-Rupture in Metals.* The MacMillan Co.: New York, 1965.

[13] S.N. Burchett, M.K. Neilsen, D.R. Frear, J.J. Stephens. *Computational continuum modelling of solder interconnects.* In R.K. Mahidhara et al., editors, Design and Reliability of Solders and Solder Interconnects, pp. 171–178, The Minerals, Metals & Materials Society, (1997).